Development of Austenitic ODS Strengthened Alloys for Very High Temperature Applications

Yinbin Miao, Kun Mo, Guangming Zhang, Bai Cui, Wei-Ying Chen, Virginia McCreary, David Gross, Ian M. Robertson, James F. Stubbins

Department of Nuclear, Plasma and Radiological Engineering

University of Illinois at Urbana-Champaign

Overview

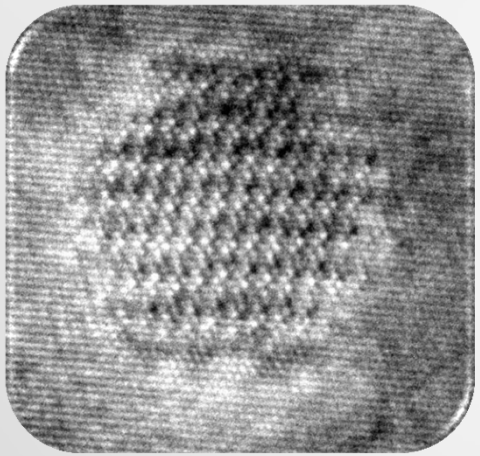

Orientation Relationship of Nanoparticles

Particle-Dislocation Interaction

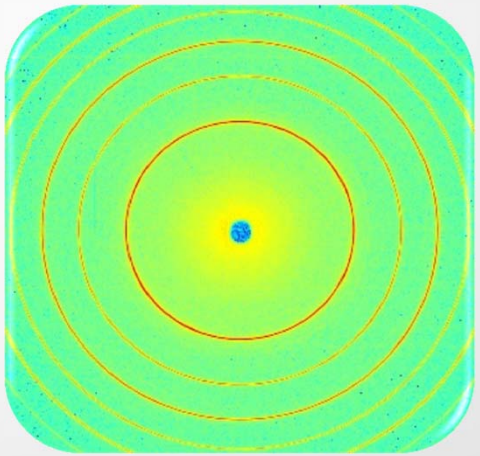

Synchrotron Radiation Studies

Challenges

- Interest in high temperature metal-base alloys for very high temperature applications – primarily driven by heat exchange and energy conversion applications in VHTRs
- Lead high temperature alloys are: Inconel 617 (Alloy 617) and Haynes 230 (Alloy 230) – based around Ni-20Cr (nichrome) – MA 754
- Proposed service conditions: temperatures up to 1000C in at moderate stresses in low or no irradiation environments with low oxidation potential and high carbon activities
- Difficulties:
  - Very low strength at temperatures above 800C, with low uniform elongation
  - Difficulty to form protective oxides; carburization and subsurface oxide formation are problematic
  - Need to characterize creep and creep-fatigue, etc.
  - Major finding: carbide restructuring and migration of carbon to grain boundaries limits elevated temperature performance (ODS is not a solution for this)

ODS PNC316 Stainless Steel

- PNC316+0.35wt%Y_2O_3+0.1wt%Ti+0.6wt%Hf, Austenite
- MA 24h→1150C, 2h→Hot Extrusion→1100C 1h
- Grain Size: 0.5~1micron

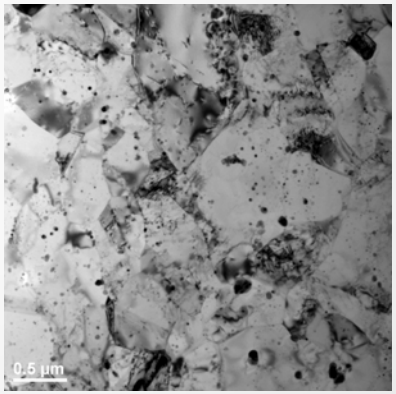

Yield Strength

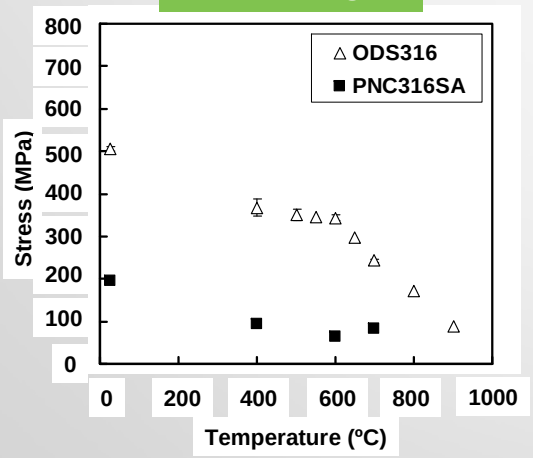

Ultimate Tensile Strength

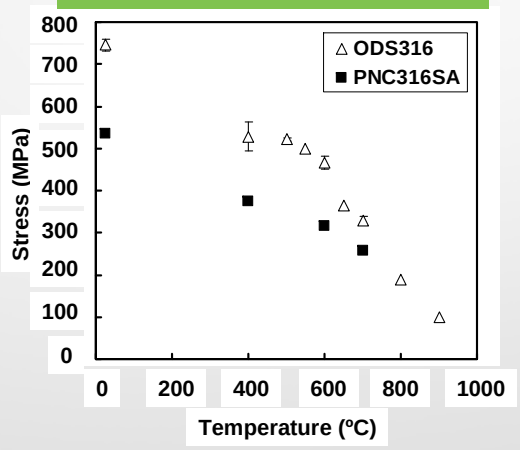

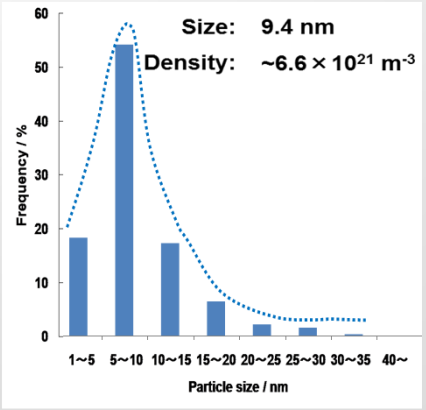

element	Fe	Cr	Ni	Mo	Mn	Ti	Si	Nb+Ta	C
wt%	bal.	16.16	13.66	2.33	1.82	0.08	0.75	0.08	0.05

Chemical Composition

- Sparse large TiC particles (>100nm) and dense oxide nanoparticles
- Y, Ti and Hf are enriched in oxide nanoparticles
- $Y_2(Hf, Ti)_2O_7$, various Hf/Ti ratio
- APT analysis is planned (November, 2013)

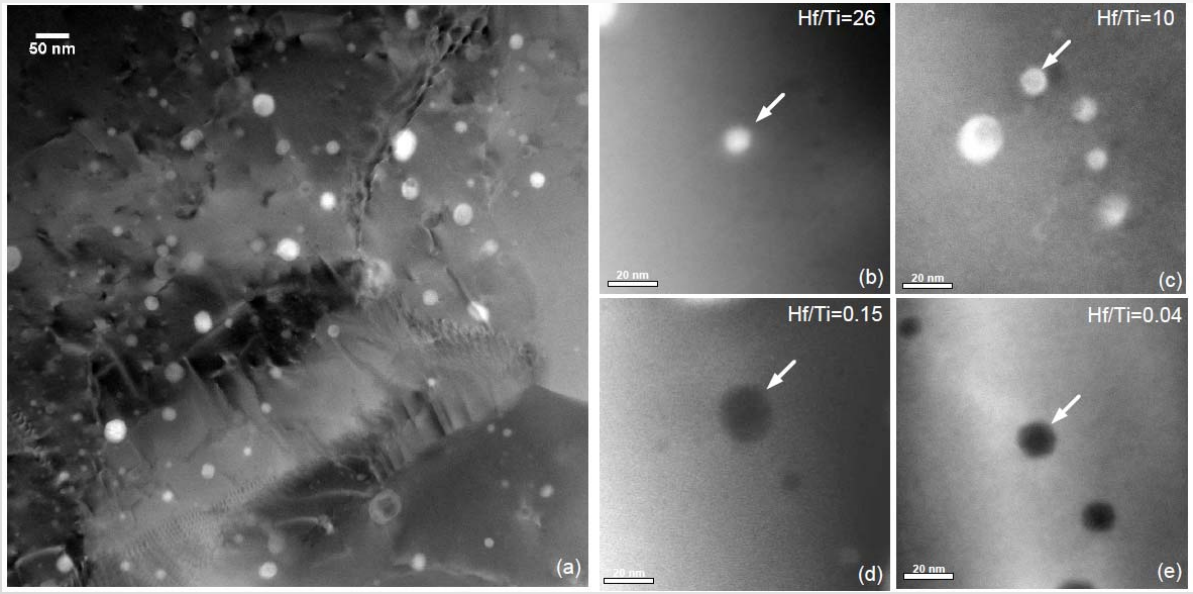

STEM-HAADF images of nanoparticles
Higher Hf/Ti ratio gives brighter Z-contrast

Synchrotron XRD of Nanoparticles

- Synchrotron XRD in APS
- 86keV monochromic X-ray
- Peaks of $Y_2(Hf, Ti)_2O_7$ and TiC were found
- Quantitative analysis shows the volume fraction of oxide particle is around 0.4%.

$$r_i = \frac{\frac{1}{n_i}\sum_{peak}\frac{I_{i,peak}}{R_{i,peak}}}{\sum_{j=\gamma,TiC,Y_2(Hf,Ti)_2O_7}\frac{1}{n_j}\sum_{peak}\frac{I_{j,peak}}{R_{j,peak}}}$$

$$R = \left(\frac{1}{v}\right)^2 FF^* p\left(\frac{1+cos^2 2\theta}{sin^2\theta cos\theta}\right)e^{-2M}$$

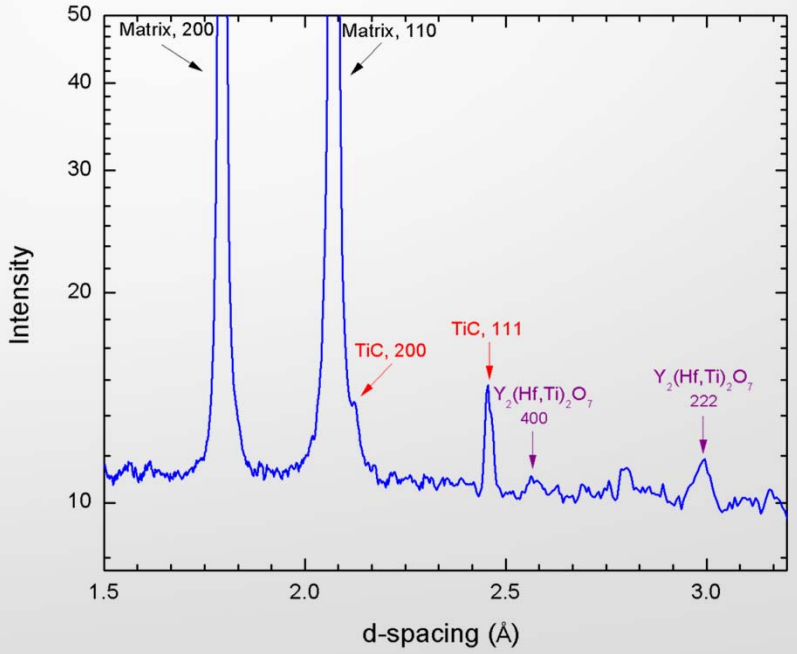

Coherent Orientation Relationship

- HREM-FFT technique was adopted
- Two different coherent orientation relations were found

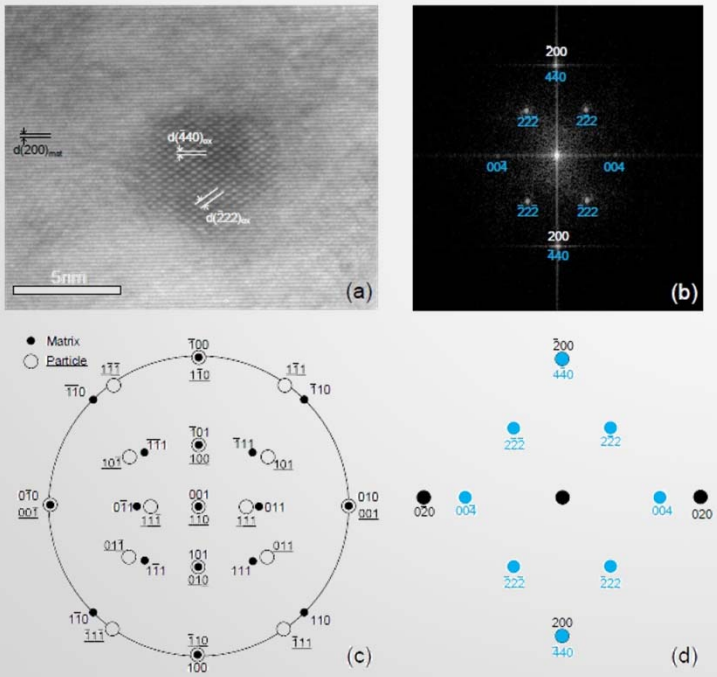

Coherency I

$(200)_{mat}//(-440)_{ox}$; $[001]_{mat}//[110]_{ox}$

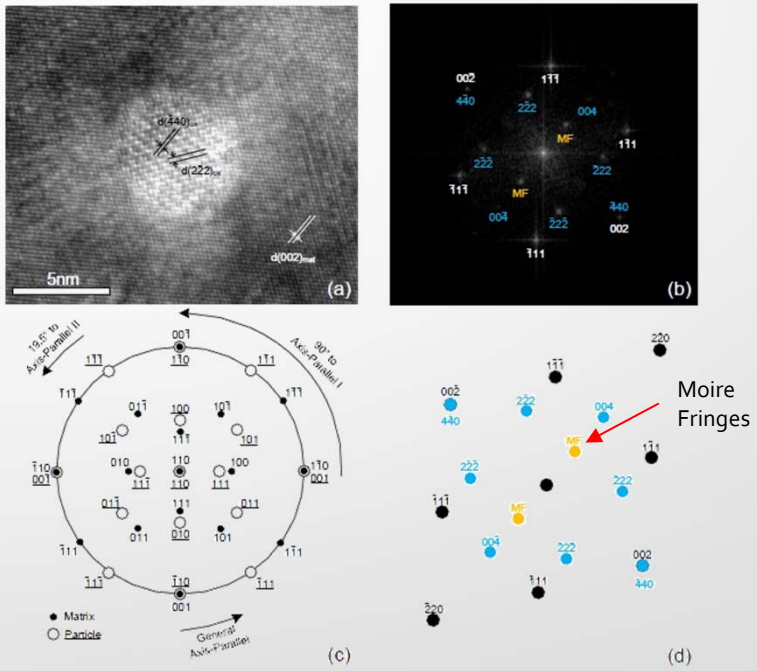

Coherency II

$(002)_{mat}//(-440)_{ox}$; $[110]_{mat}//[110]_{ox}$

Axis-Parallel Relations

- Multiple $[110]_{mat}//[110]_{ox}$ relations exist; no parallel planes with small misfit
- Two special cases: cubic-on-cubic and $[1\text{-}11]_{mat}//[\text{-}11\text{-}1]_{ox}$
- Dense dislocations due to large misfit between $\{111\}_{mat}$ and $\{222\}_{ox}$

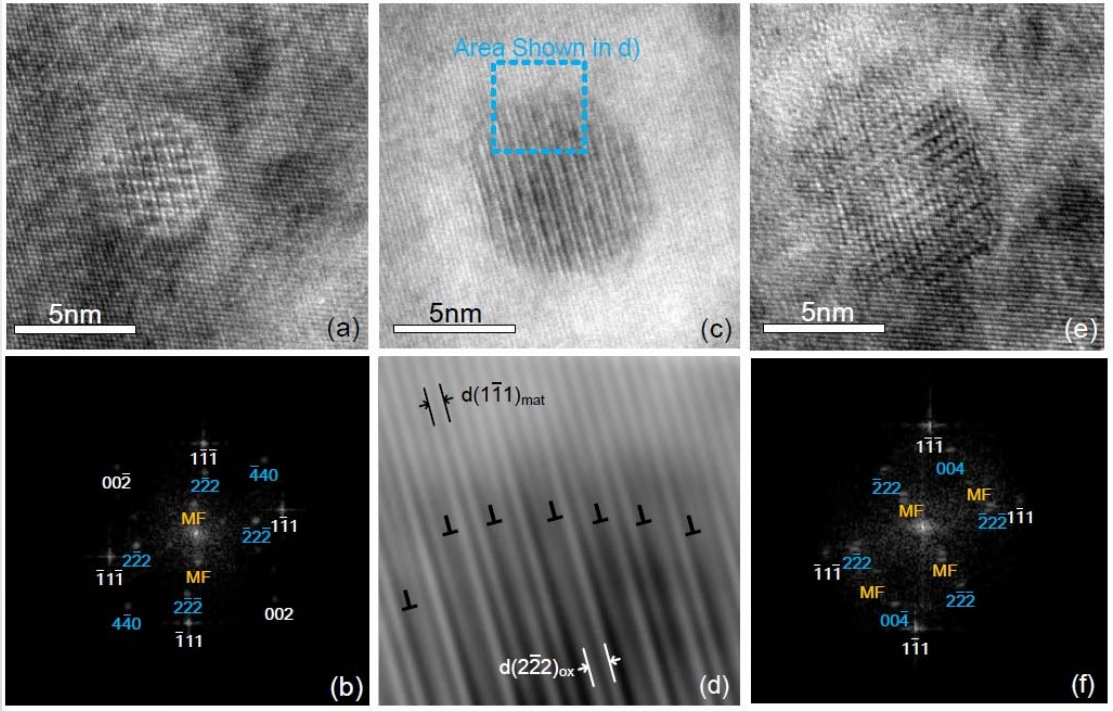

Cubic-on-cubic

Dense misfit dislocations

$[110]_{mat}//[110]_{ox}$
$[1\text{-}11]_{mat}//[\text{-}11\text{-}1]_{ox}$
Axis-parallel

Orientation Relation Evolution

- Prominent relation between particle size and orientation relationship
- Thermodynamically, surface energy (r^2) dominates small particles while strain energy (r^3) dominates large particles. So, coherent/axis-parallel small particles and randomly oriented large particles have lower energies.
- Kinetically, orientation relation of large particles needs longer time to evolve (diffusion).
- Axis-parallel relations are intermediate states during the formation of coherency according to both energy and kinetics concerns.

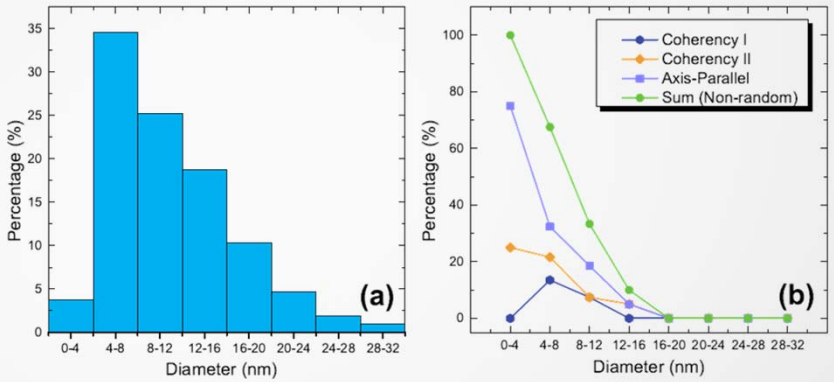

Size distribution and orientation relation percentage of oxide nanoparticles

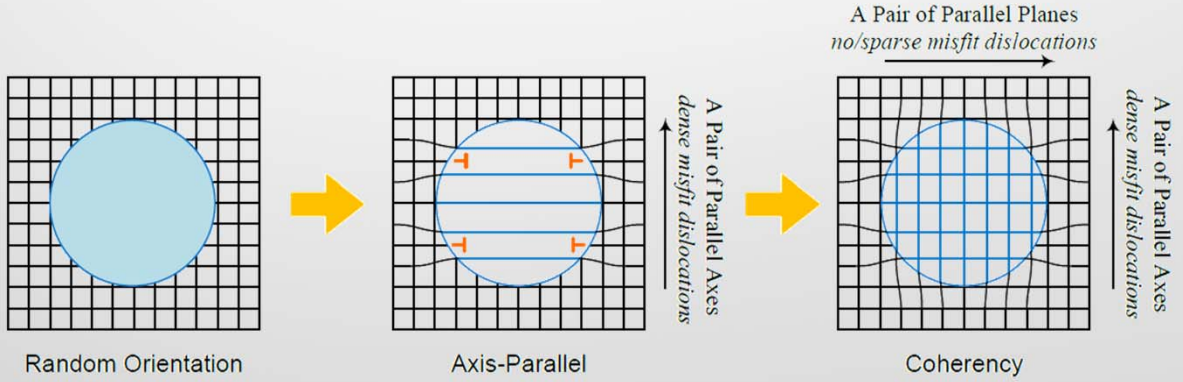

Evolution route of orientation relationship

Slip System in ODS 316 Steel

- {111}<1-10> slip system, almost pure screw dislocations
- Dissociated to two Schockley partials:

$$\frac{1}{2}\langle 01\text{-}1\rangle \rightarrow \frac{1}{6}\langle \text{-}12\text{-}1\rangle + \frac{1}{6}\langle 11\text{-}2\rangle$$

- Common for fcc materials

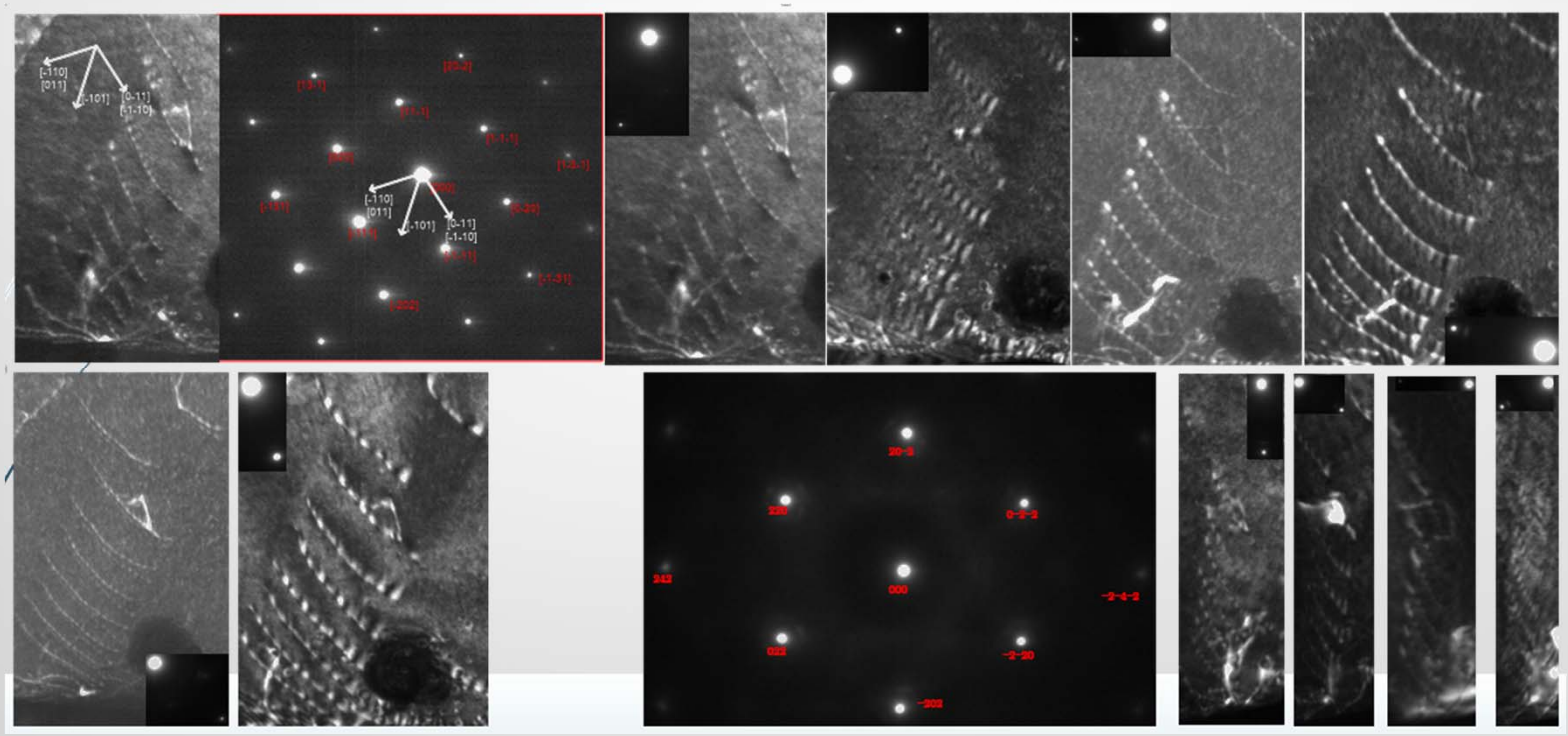

g•b characterization showing the visibility of two partials and the stacking fault in various diffraction conditions

Particle-Dislocation Interaction

- Room temperature
- Orowan mechanism was observed
- The two dissociated partials pass the particle one by one.
- Different dislocation shapes as the particle is near the center or the edge of the slip plane

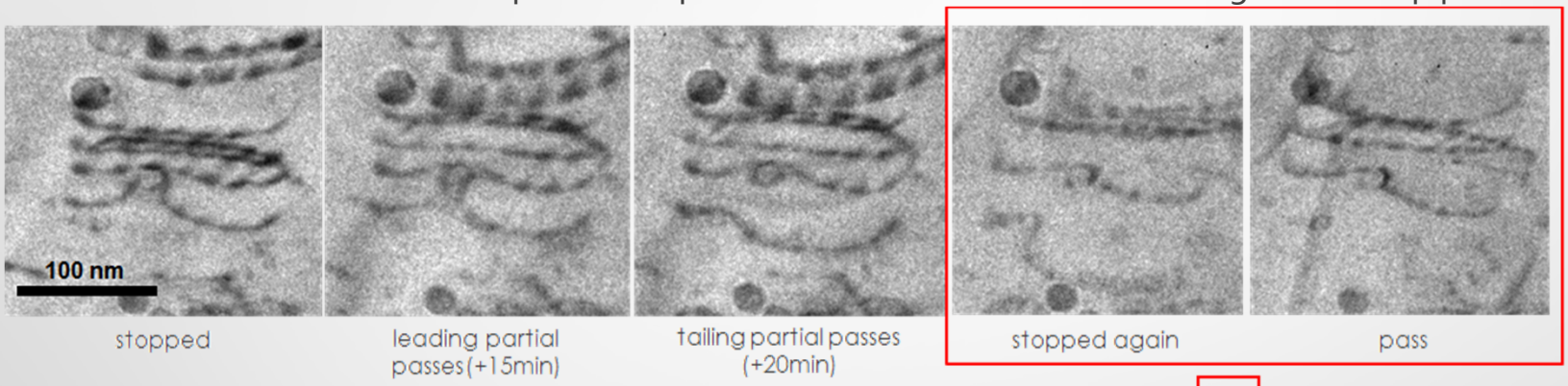

- As the particle stops the dislocation near the edge of the slip plane, the dislocation becomes z-shape after passing the particle and recovers its line-shape during further gliding.

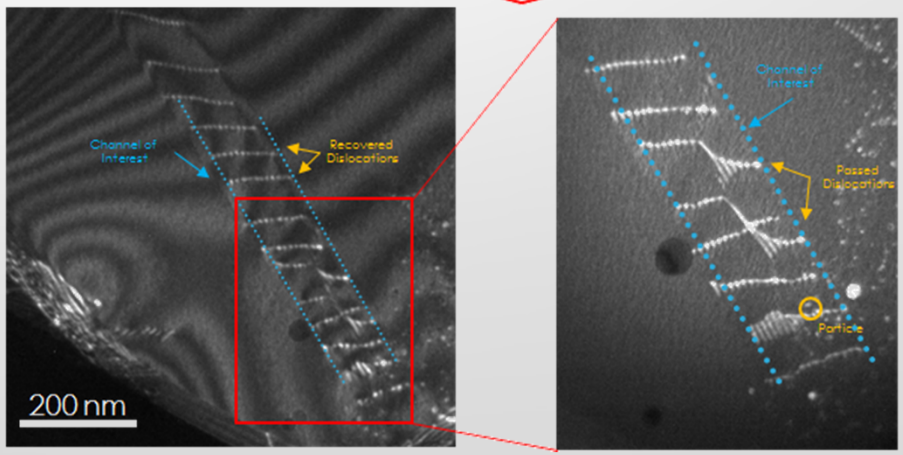

Dislocation shape evolution after passing a particle near the edge of its slip plane

Particle-Dislocation Interaction

- As one slip channel is stopped by particles, new channels will be activated.
- Some of new channels will also be stopped by particles.
- Dislocations keep gliding in activated channels to help release the local stress.
- Higher efficiency of particles are needed for better performances.

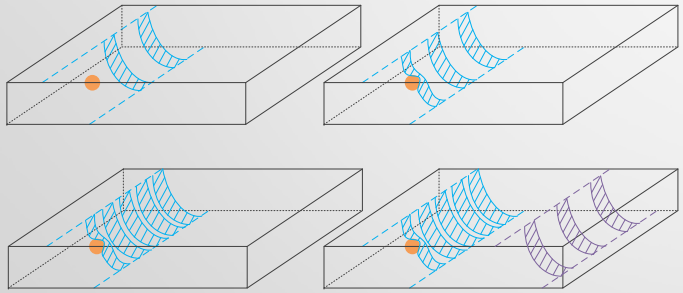

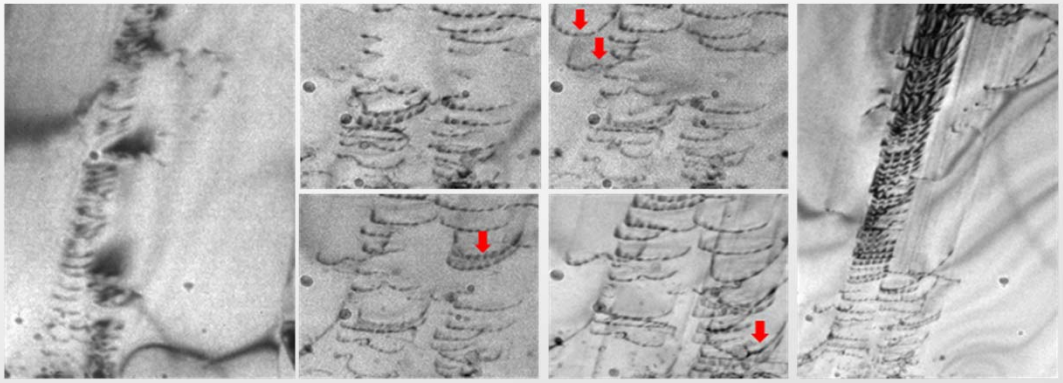

Beginning: only one activated slip channel

Multiple channels were activated after the original channel was stopped by particles

End: dislocations piled up in the stopped channel

Evolution of slip channels after the original channel is suppressed by oxide particles

Conclusions: ODS 316 Steel

- Oxide particles are $Y_2(Hf,Ti)_2O_7$ (STEM/EDS, synchrotron and electron diffraction)
- 2 coherent orientation relations, a series of axis-parallel relations
- Orientation relationship is highly correlated to the size of the oxide particle.
- The small oxide particles evolve to coherency via diffusion, with axis-parallel relations as intermediate states.
- The primary slip system is {111}<1-10> with almost pure screw dislocations dissociated into pairs of Shockley partials.
- Orowan mechanism was found in particle-dislocation interaction.
- New slip channels are activated to release local stress as previously formed channels are suppressed by particles.

Synchrotron Radiation Study

- Sector 1-ID beamline at the Advanced Photon Source
- X-ray energy: 86 keV (λ=0.0144nm)
- Beam size: 300×300 μm²

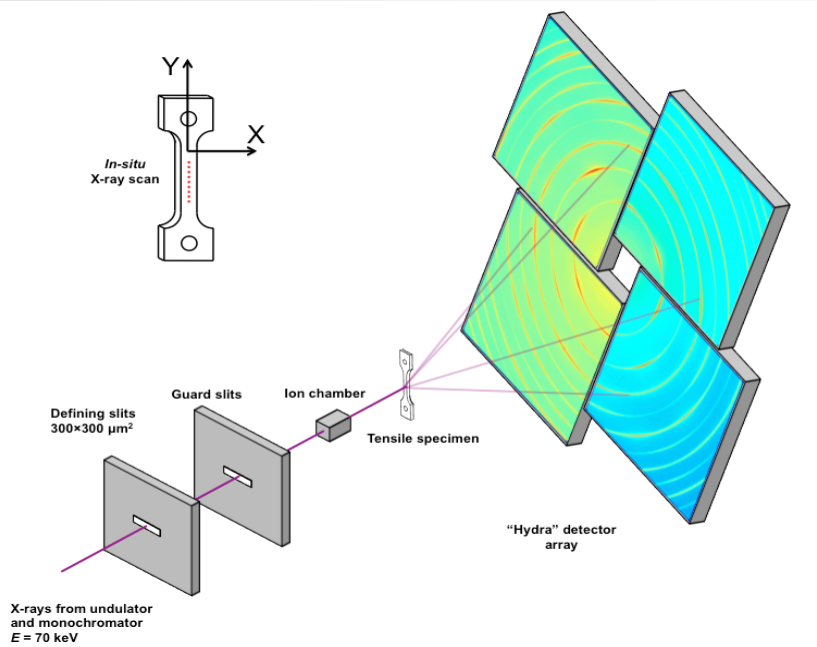

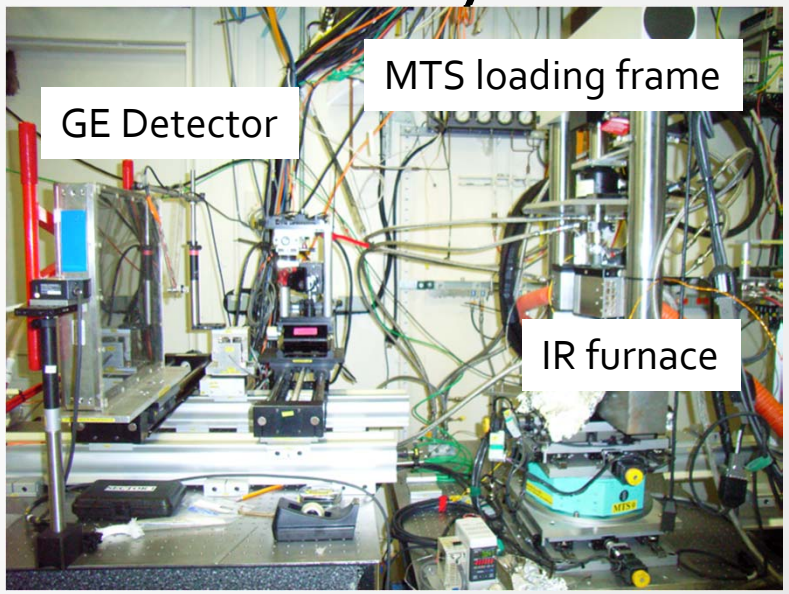

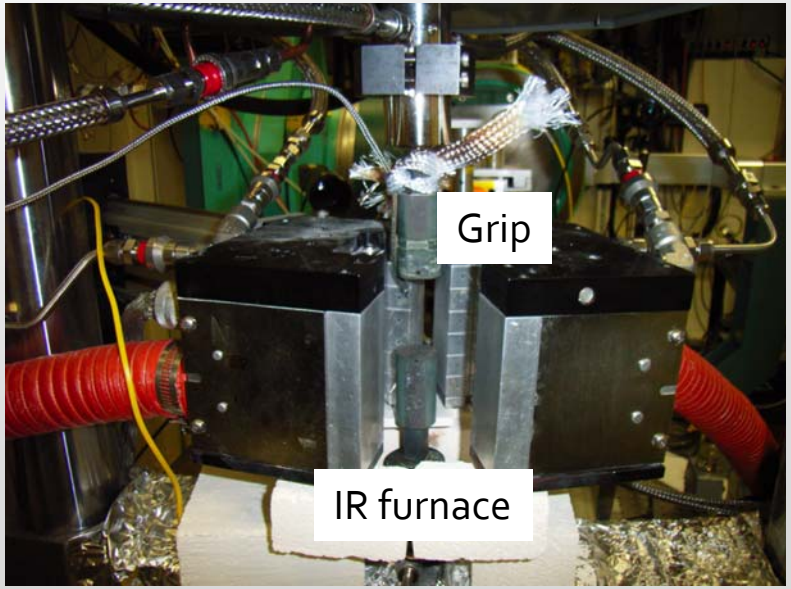

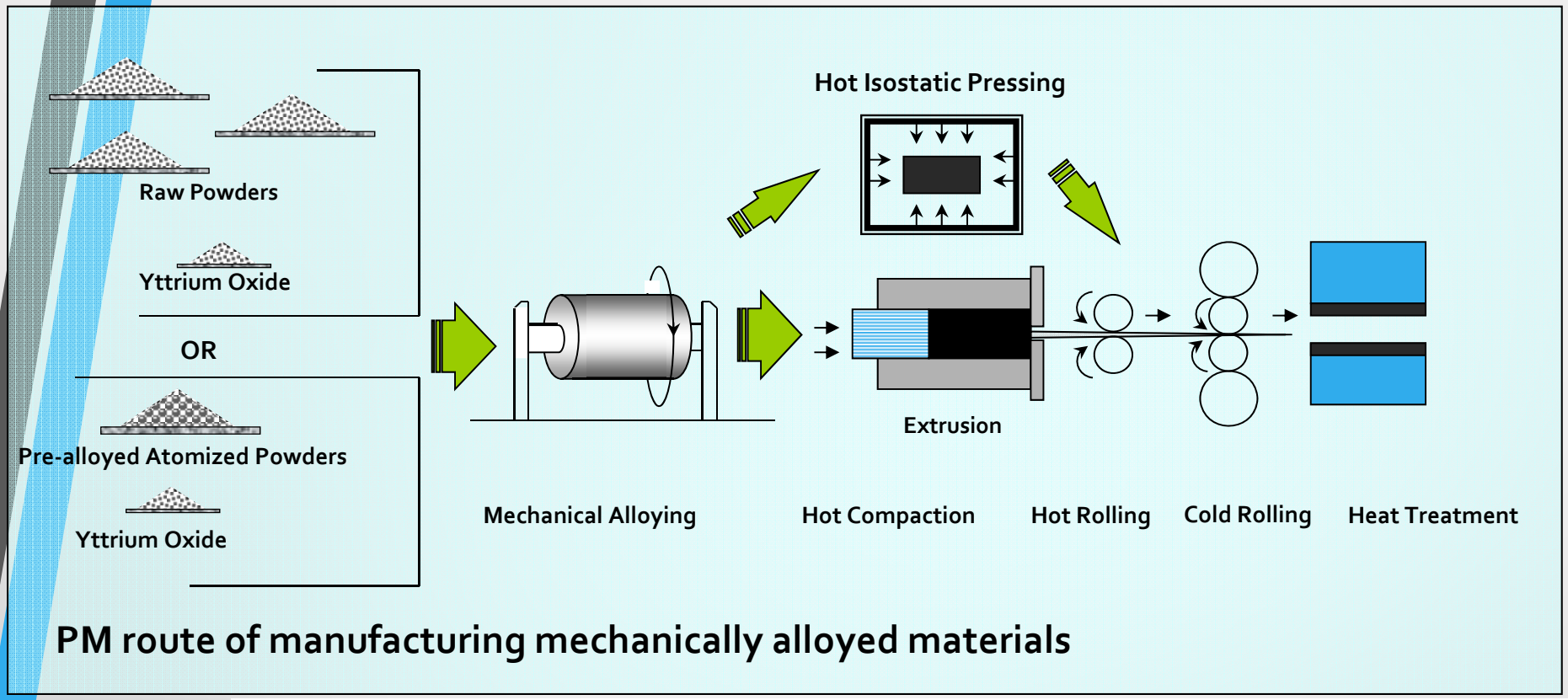

PM route of manufacturing mechanically alloyed materials

Austenitic ODS Steels

Alloys	Fe	Ni	Cr	W	V	Ti	Si	Al	Mo	Nb/Ta	Mn	C	Y_2O_3
316 ODS	bal.	13.7	16.2	-	-	0.08	0.75	-	2.3	0.08	1.3	-	0.35
304 ODS	bal.	8	18	-	-	0.5	0.15	-	1	-	-	-	0.35
310 ODS	bal.	20	25	-	-	0.5	-	-	1	-	-	-	0.35
MA 754	-	bal.	20	-	-	0.5	-	0.3	-	-	-	0.05	0.6

Ferritic ODS Steels

Alloys	Fe	Cr	W	V	Ti	Si	Al	Mo	Mn	C	Y_2O_3
9 Cr ODS	bal.	12	1.5	0.2	0.5	-	-	-	-	0.1	0.35
12 Cr ODS	bal.	12	1.2	-	0.5	0.15	-	-	0.5	0.1	0.35
14 Cr ODS	bal.	14	2	-	0.5	0.15	-	-	-	-	0.35
18 Cr ODS	bal.	18	2	-	0.5	0.15	4	-	-	-	0.35
MA 957	bal.	14	-	-	0.9	-	-	0.3	-	0.01	0.25

Synchrotron In-situ and Ex-situ Experiment

- In-situ experiment:
  - Austenitic: MA 754 ; 304 ODS
  - Ferritic: 9 Cr ODS; 12 Cr ODS; 14 Cr ODS; 18 Cr ODS
- En-situ experiment:
  - Austenitic: 316 ODS
  - Ferritic: Aged 9 Cr ODS; 12-18 Cr ODS with different % of Ti and Al
- Temperature: room temperature, 300°C, 500°C, 600°C, and 700°C

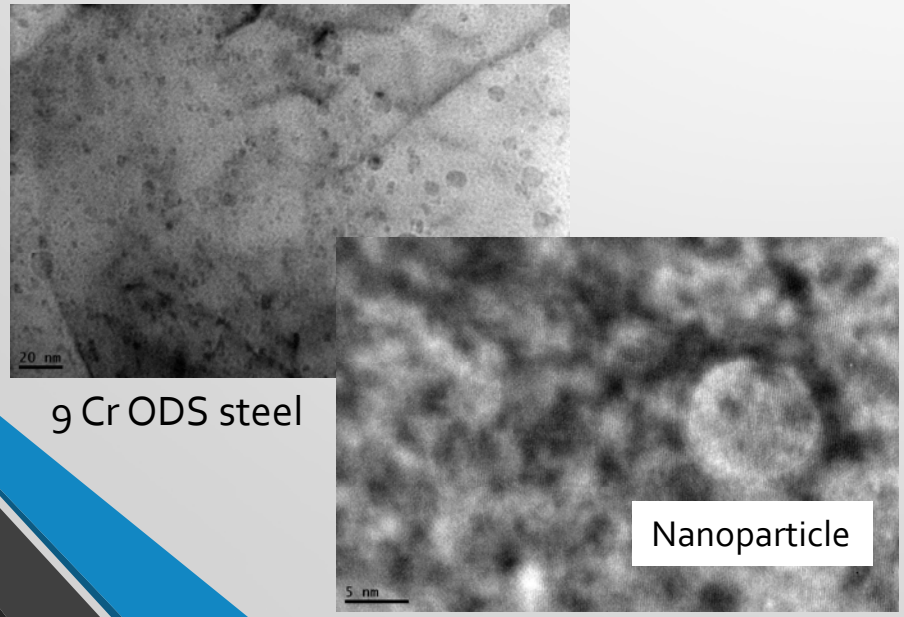

9 Cr ODS steel

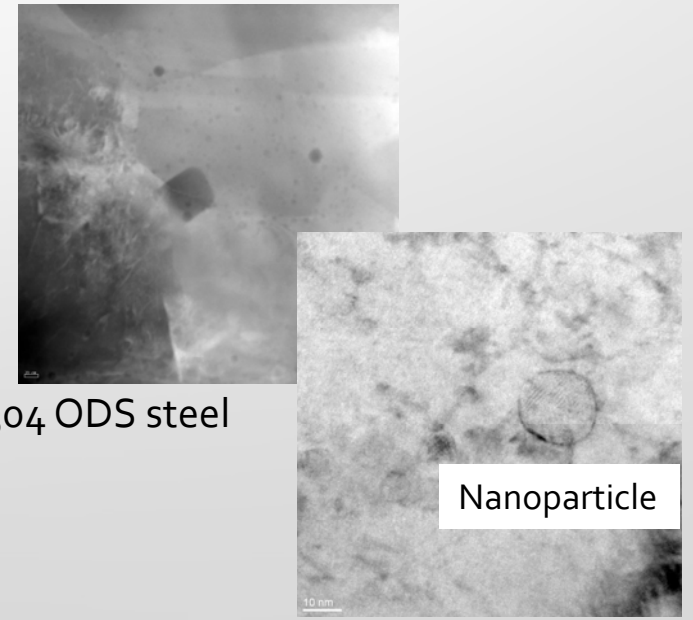

304 ODS steel

Example: 9Cr ODS steel

- Three major phases observed by electron microscopies were also found using synchrotron X-ray diffraction
- All of the diffraction peaks were identified; the most significant reflections of $Y_2Ti_2O_7$ are (222) and (440) reflections with d-spacings of ~2.91 and 1.78Å, respectively; the corresponding value of the lattice constant is ~10.09 Å

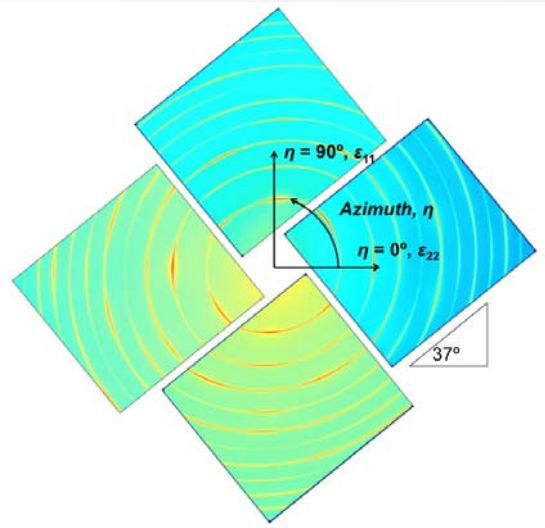

F/M Matrix, BCC structure		TiN, FCC structure		$Y_2Ti_2O_7$, FCC structure	
hkl	*d*-space (Å)	*hkl*	*d*-space (Å)	*hkl*	*d*-space (Å)
110	2.029	111	2.449	222	2.915
200	1.435	200	2.122	400	2.519
211	1.172	220	1.499	331	2.306
220	1.015	311	1.279	440	1.784
310	0.9072	222	1.224	622	1.52
222	0.828	400	1.06		
321	0.7665	331	0.973		
400	0.7171	420	0.948		
330/411	0.6765	422	0.8657		
420	0.6414	511/333	0.8161		

X-ray diffraction pattern of the 9 Cr ODS steel

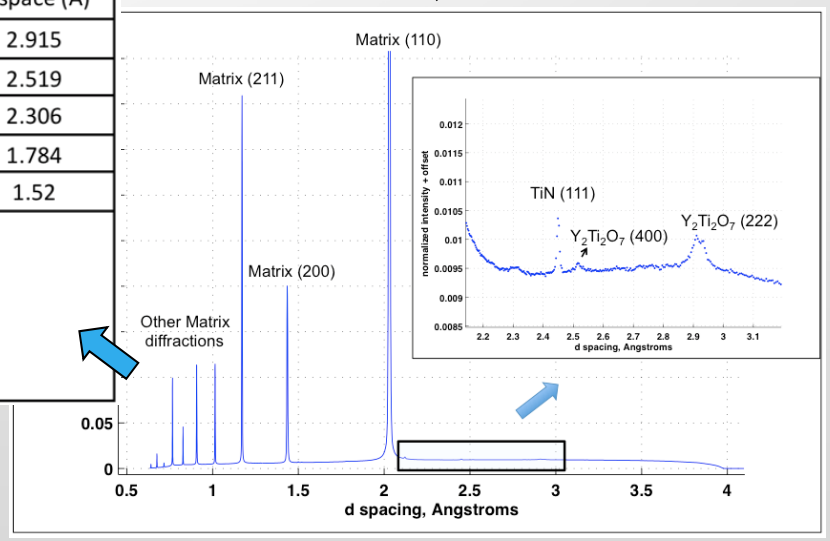

The stress-strain diagram of 9 Cr ODS sample

- Young's modulus: ~203 GPa
- 0.2% yield strength: ~845 MPa
- Ultimate tensile strength (UTS): ~ 915 MPa, at the strain of ~8.6%
- Total elongation: ~16.2%

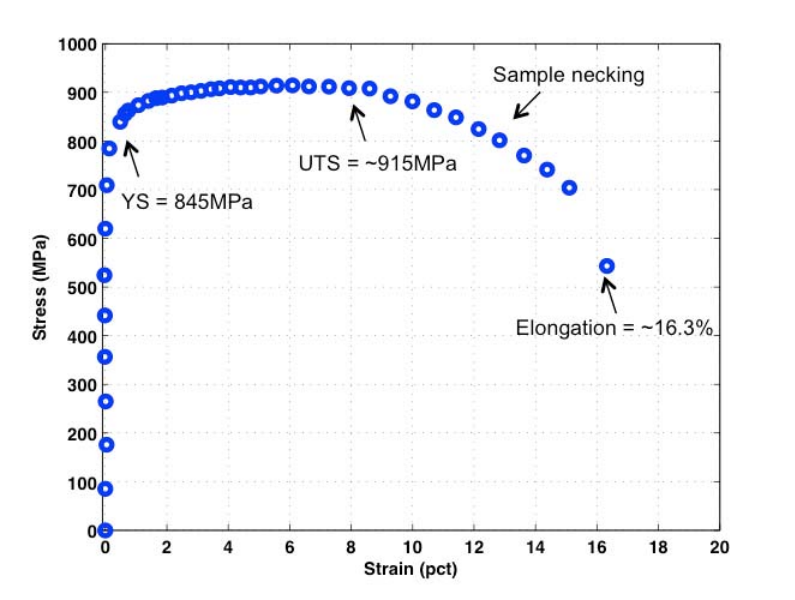

Engineering stress vs. Strain

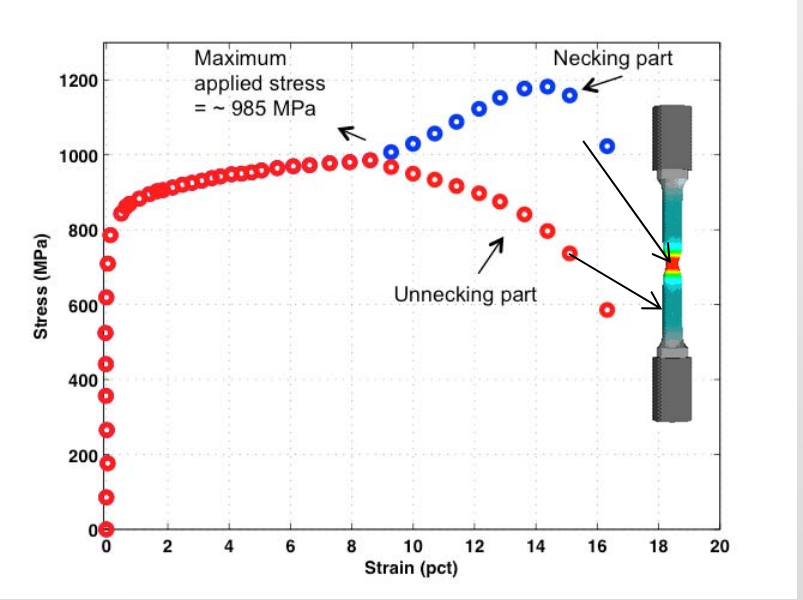

True stress vs. strain

Load Partitioning of 9 Cr ODS sample

- Load partitioning during plastic deformation
  - Significant load placed on the nanoscale Y2Ti2O7 particles
  - F/M matrix is slightly relaxed after sample yielding

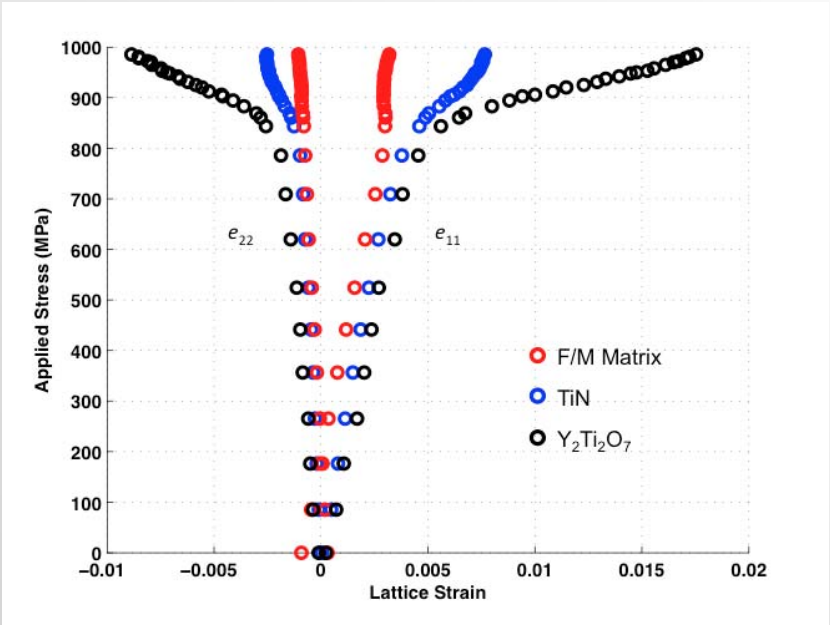

Applied stress vs. lattice strain for F/M matrix (321) reflection $Y_2Ti_2O_7$ (222) reflection, and TiN (111) reflection in the 9Cr ODS steel

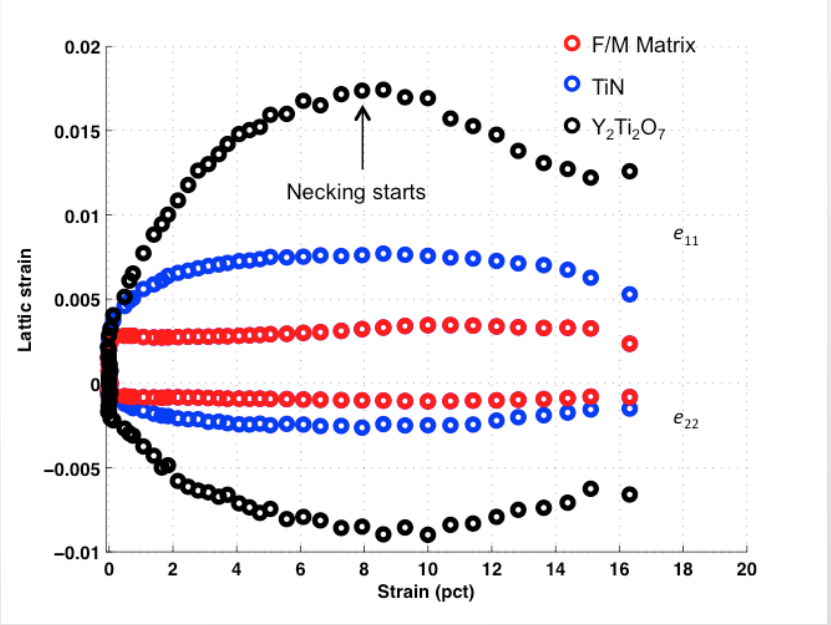

Lattice stress vs. macroscopic strain for F/M matrix (321) reflection $Y_2Ti_2O_7$ (222) reflection, and TiN (111) reflection in the 9Cr ODS steel

Necking Part vs. Unnecking Part

- X-ray scanning along the gauge part of the specimen:
  - two scan points (point #4 and #5) were placed on the necking part
  - seven other points were placed on the unnecking part of the sample
- For matrix and particles, different lattice strain development were observed for necking and unnecking parts during plastic deformation

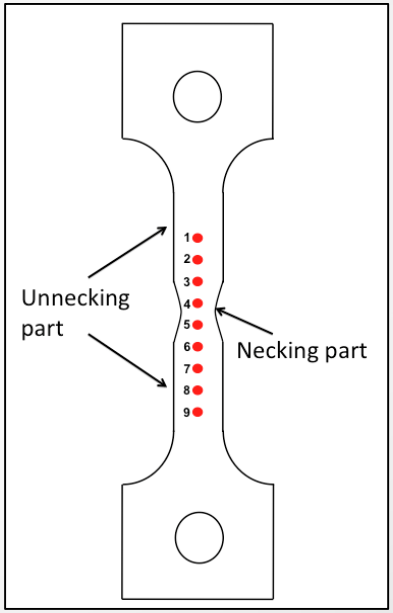

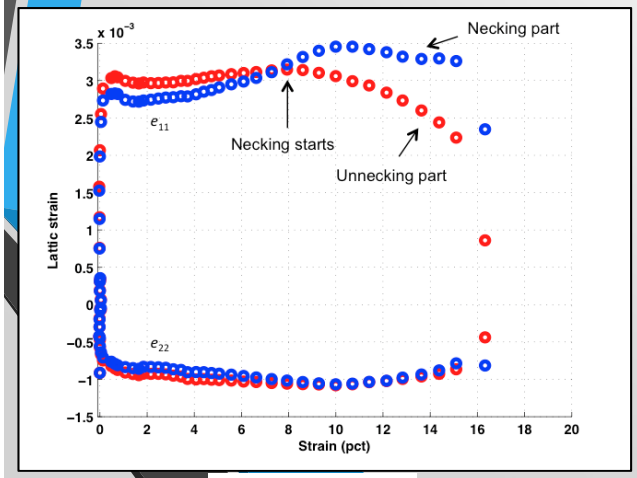

F/M matrix

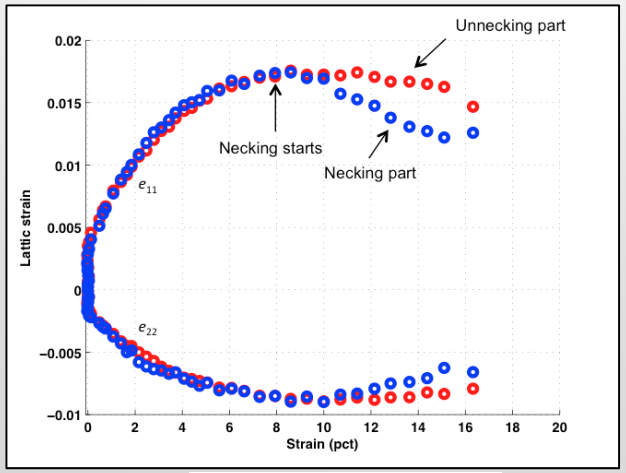

Y2Ti2O7 particles

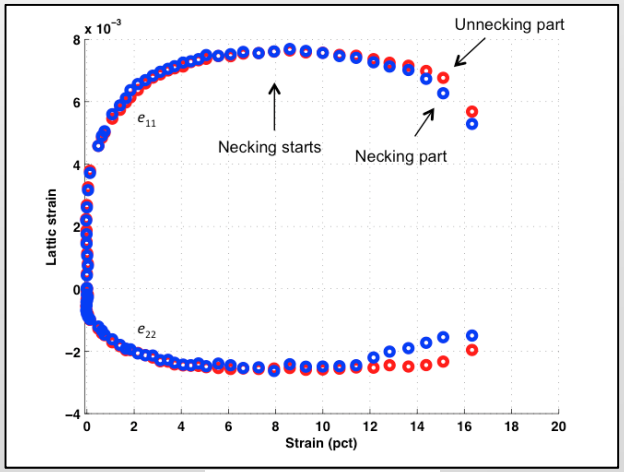

TiN particles

Necking Part vs. Unnecking Part for F/M matrix

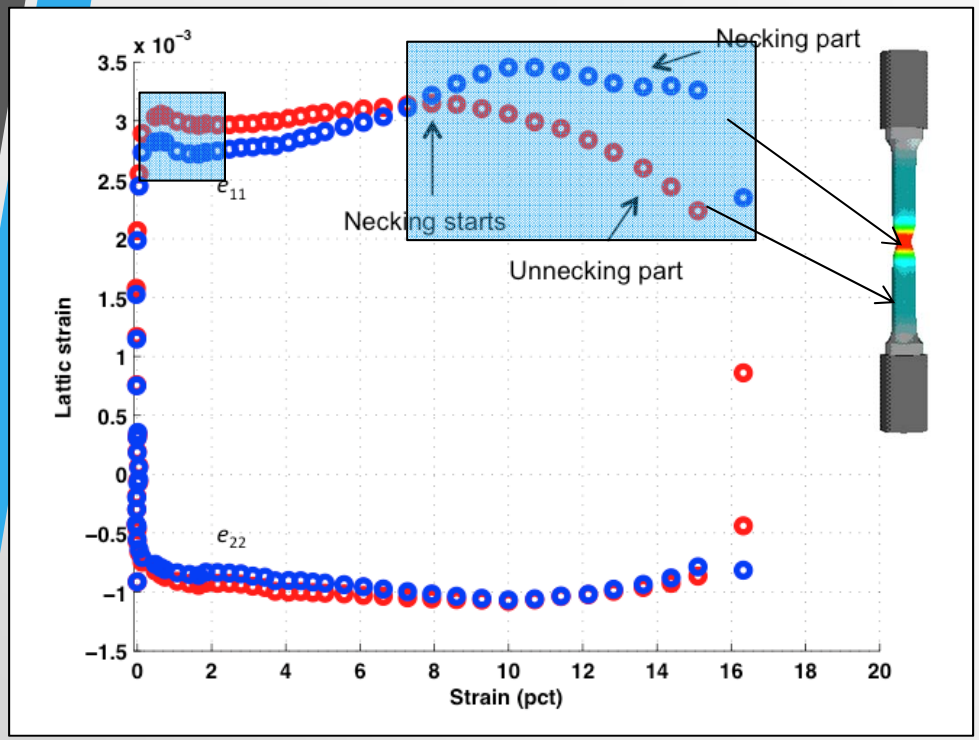

Lattice stress vs. macroscopic strain for F/M matrix (321) reflection

- The area withstand low load during early yielding is the area of necking

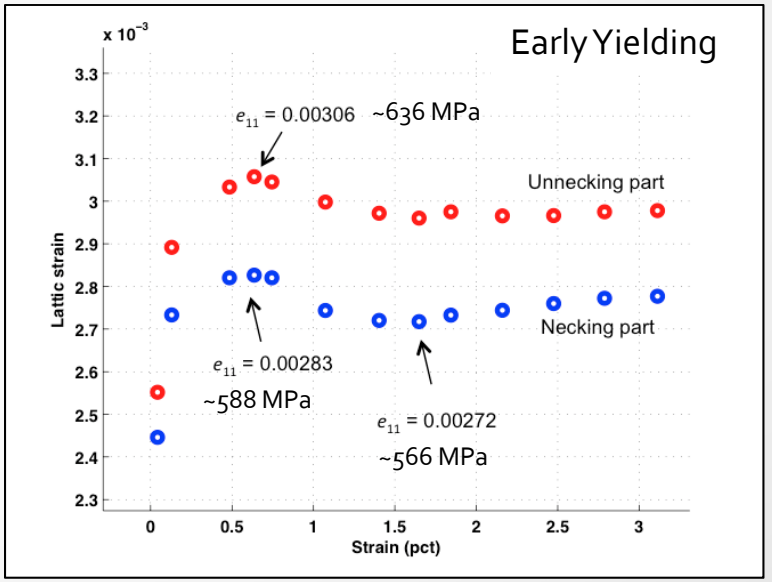

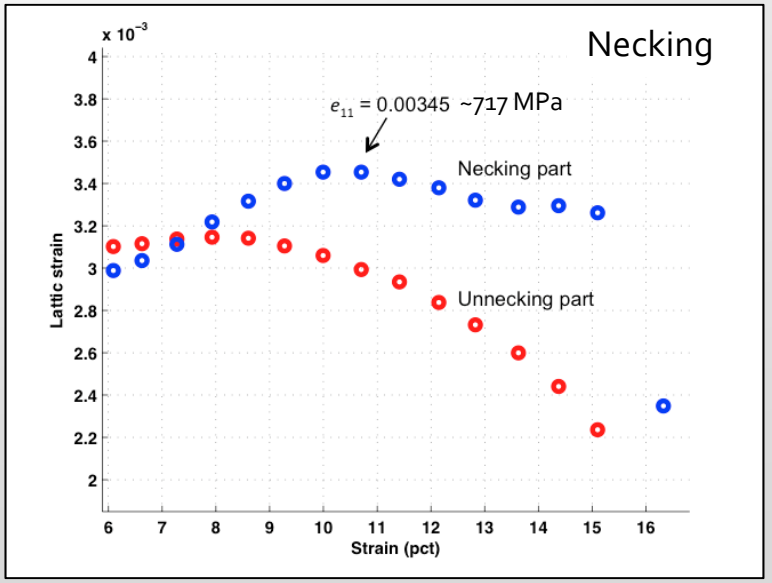

Necking Part vs. Unnecking Part for Nanoparticles

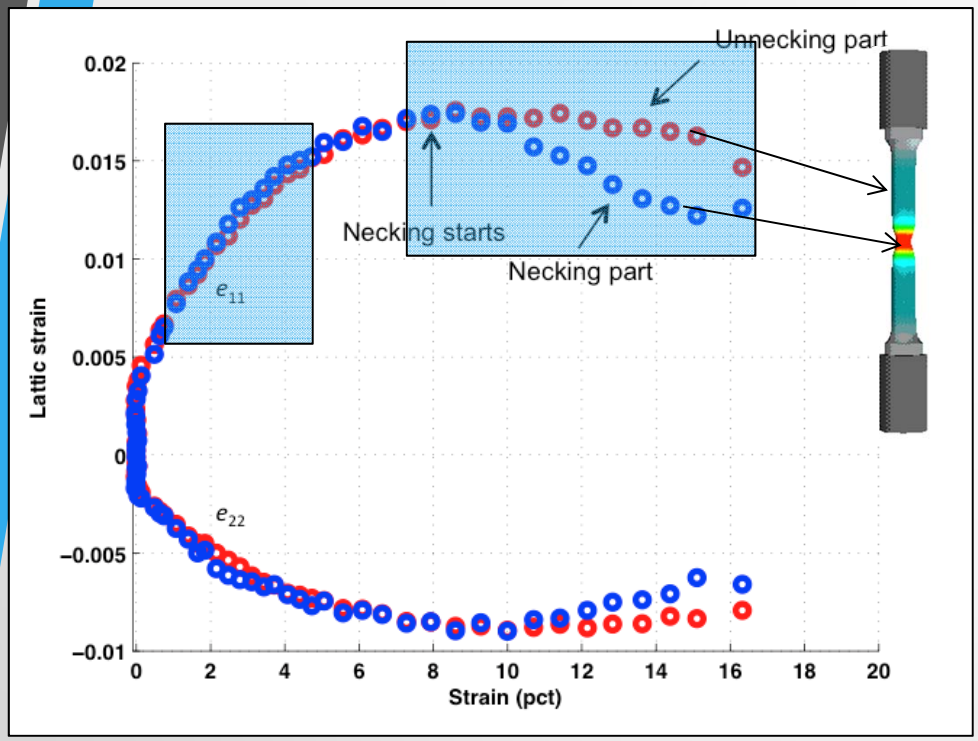

Lattice stress vs. macroscopic strain $Y_2Ti_2O_7$ (222) reflection

- The area withstand high load during early yielding is the area of necking
- Large straining (also large internal stress) causes particle decohesion from the matrix

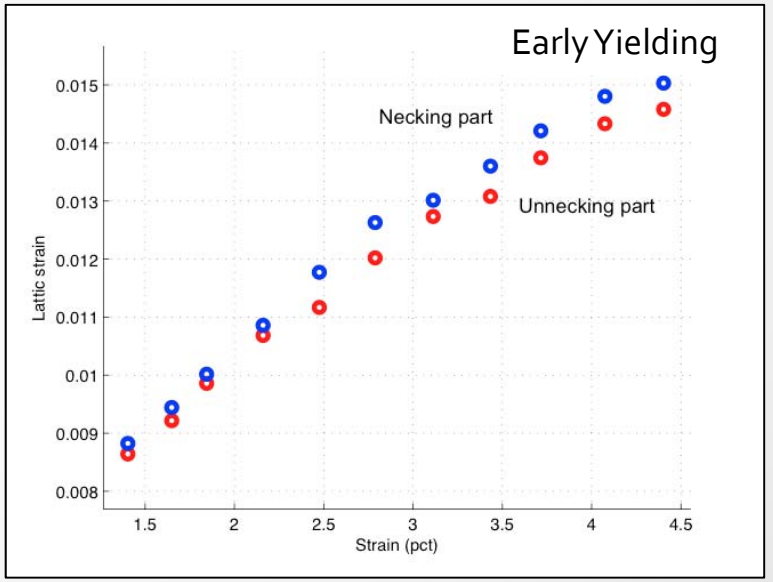

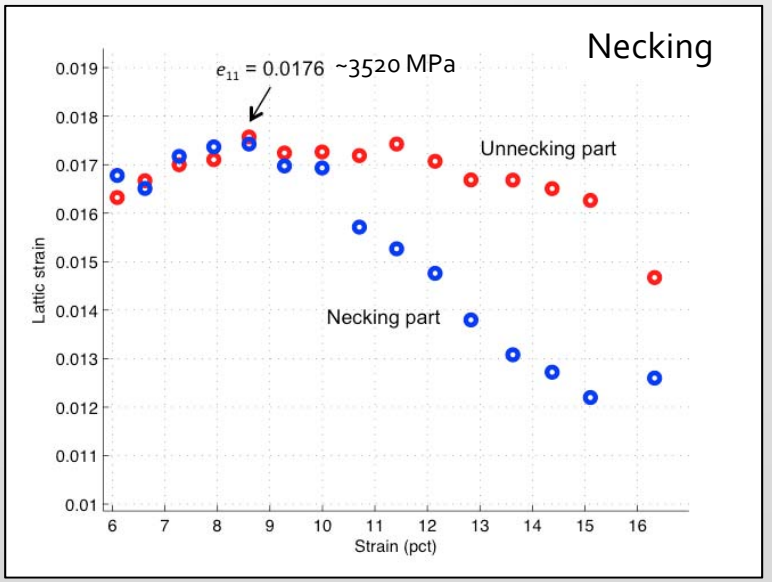

Conclusions: 9Cr ODS WAXS study

- Load partitioning between the ferritic matrix and the nanoparticles during sample yielding
- The impact of $Y_2Ti_2O_7$ particles is limited in elastic and plastic deformations to before necking, with a maximum internal stress of **~3.5 GPa** (corresponding to a lattice strain of 0.0176).

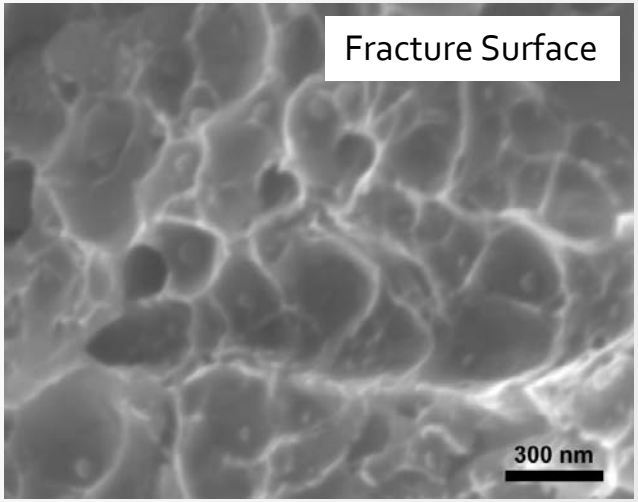

Before necking, macroscopic strain: 0-8.6%				
Phases	Maximum values		Average values	
	$\sigma_{11}^{necking} - \sigma_{11}^{unnecking}$	$e_{11}^{necking} - e_{11}^{unnecking}$	$\sigma_{11}^{necking} - \sigma_{11}^{unnecking}$	$e_{11}^{necking} - e_{11}^{unnecking}$
F/M matrix	-52MPa	-2.5×10^{-4}	-25MPa	-1.2×10^{-4}
$Y_2Ti_2O_7$	122MPa	6.1×10^{-4}	44MPa	2.2×10^{-4}
TiN	66MPa	2.9×10^{-4}	22MPa	9.8×10^{-5}
After necking, macroscopic strain: 8.6-16.3%				
Phases	Maximum values		Average values	
	$\sigma_{11}^{necking} - \sigma_{11}^{unnecking}$	$e_{11}^{necking} - e_{11}^{unnecking}$	$\sigma_{11}^{necking} - \sigma_{11}^{unnecking}$	$e_{11}^{necking} - e_{11}^{unnecking}$
F/M matrix	213MPa	1.0×10^{-3}	142MPa	6.8×10^{-4}
$Y_2Ti_2O_7$	-812MPa	-4.1×10^{-3}	-450MPa	-2.3×10^{-3}
TiN	-112MPa	-4.9×10^{-4}	-21MPa	-9.1×10^{-5}

Further study

- Orientation relationship of oxide nanoparticles
  - FEM and analytic description of stress field around the nanoparticle
  - Atom probe tomography (APT)
  - More austenitic ODS alloys: MA754, ODS 304, ODS 310
- Particle-dislocation interaction
  - Other mechanisms, especially for the small coherent nanoparticles
  - Mechanisms at various temperatures
- Synchrotron radiation analysis of austenitic ODS steels:
  - Particle-matrix orientation relation analysis based on synchrotron diffraction patterns
  - Load partitioning and particle responses for ODS steels at elevated temperatures
  - Load partitioning and particle responses for ODS steels after thermal aging
- Biaxial Creep behavior for ODS steels: pressurized creep tube study
- Materials Production